SUTURED FLOER HOMOLOGY AND HYPERGRAPHS

ANDRÁS JUHÁSZ, TAMÁS KÁLMÁN, AND JACOB RASMUSSEN

ABSTRACT. By applying Seifert's algorithm to a special alternating diagram of a link L, one obtains a Seifert surface F of L. We show that the support of the sutured Floer homology of the sutured manifold complementary to F is affine isomorphic to the set of lattice points given as hypertrees in a certain hypergraph that is naturally associated to the diagram. This implies that the Floer groups in question are supported in a set of Spin^c structures that are the integer lattice points of a convex polytope. This property has an immediate extension to Seifert surfaces arising from homogeneous link diagrams (including all alternating and positive diagrams).

In another direction, together with work in progress of the second author and others, our correspondence suggests a method for computing the "top" coefficients of the HOMFLY polynomial of a special alternating link from the sutured Floer homology of a Seifert surface complement for a certain dual link.

1. INTRODUCTION

In this paper, we report on an unexpected coincidence between two sets of integer lattice points that appear in the study of alternating links and their Seifert surfaces. The first set derives from the first author's sutured Floer homology theory [9]. Given a link $L \subset S^3$ with Seifert surface F, we can associate to it the sutured Floer homology group $SFH(S^3 - F, L)$, where $(S^3 - F, L)$ is the sutured manifold complementary to F. This group decomposes as a direct sum over relative Spin^c structures on $(S^3 - F, L)$, namely,

$$SFH(S^3 - F, L) = \bigoplus_{\mathfrak{s} \in \mathrm{Spin}^c(S^3 - F, L)} SFH(S^3 - F, L, \mathfrak{s}).$$

The set $\mathrm{Spin}^c(S^3 - F, L)$ of relative Spin^c structures can be thought of as an affine copy of $H_1(S^3 - F; \mathbf{Z})$. The *support*

$$S(F) = \{\, \mathfrak{s} \in \mathrm{Spin}^c(S^3 - F, L) \mid SFH(S^3 - F, L, \mathfrak{s}) \neq 0 \,\}$$

carries a lot of interesting geometric information about F, see [10, 11, 12].

A priori, $SFH(S^3 - F, L, \mathfrak{s})$ is a $\mathbf{Z}/2\mathbf{Z}$ graded group. However, if L is a non-split alternating link and F is an arbitrary minimal genus Seifert surface of L, then by [5, Corollary 6.11], each group $SFH(S^3 - F, L, \mathfrak{s})$ is either trivial or isomorphic to $\mathbf{Z}$, and all nontrivial groups have the same $\mathbf{Z}/2\mathbf{Z}$ grading. Thus, in this case, $SFH(S^3 - F, L)$ is determined by $S(F)$. Furthermore, we see that $S(F)$ may be

Key words and phrases. Alternating link, Seifert surface, Floer homology, integer polytope, hypergraph.

AJ was supported by a Royal Society Research Fellowship and OTKA grant NK81203.

TK was supported by the Japan Society for the Promotion of Science (JSPS) Grant-in-Aid for Young Scientists B, no. 21740041.

viewed as the Euler characteristic (function) $\chi(\mathfrak{s}) = \chi(SFH(S^3 - F, L, \mathfrak{s}))$. Indeed, up to an overall sign, χ agrees with the indicator function of $S(F)$.

The second set was introduced by A. Postnikov [17] and (independently, but later) by the second author [13], who based on it a new theory of polynomial invariants of bipartite graphs and hypergraphs. Its elements are generalized spanning trees called hypertrees. More precisely, if $\mathcal{H} = (V, E)$ is a hypergraph with vertex set V and hyperedge set E (i.e., V is a finite set and E is a finite multiset of subsets of V), then an obvious two-to-one correspondence associates to it the bipartite graph $\operatorname{Bip}\mathcal{H}$ with color classes E and V. Now a hypertree in $\mathcal{H}$ is a vector $\mathbf{f}\colon E \to \mathbf{N} = \{0, 1, 2, \dots\}$ so that $\operatorname{Bip}\mathcal{H}$ has a spanning tree with valence $\mathbf{f}(e) + 1$ at every $e \in E$. The set of all hypertrees in $\mathcal{H}$ will be denoted by[1] $Q_{\mathcal{H}} = Q_{(V,E)}$.

To place the support S of SFH and the set of hypertrees Q in the same context, recall that to any plane graph G we may associate an alternating link L_G and a surface F_G. The latter is obtained by taking a regular neighborhood of G and inserting a twist over each edge; L_G is its boundary. This is also known as the median construction on G. When G is bipartite, L_G is naturally oriented so that F_G is its Seifert surface. The class of oriented links that arise as L_G for some bipartite plane graph G is called *special alternating*, and it is known that F_G is of minimal genus among Seifert surfaces of L_G. (Here, we allow multiple edges in G.) Let R denote the set of connected components (regions) of $S^2 - G$ and let (E, R) be the hypergraph where $r \in R$ contains all elements of E that lie along ∂r. Define (V, R) similarly. (We will soon shift the meaning of r from region to a point marking the region, and thus R will mean the set of those points.) Note that $S^3 - F_G$ is a handlebody of genus $|R| - 1$. Our main result is the following.

Theorem 1.1. *Let G be a plane bipartite graph with color classes E, V and regions R. Then*

$$S(F_G) \cong Q_{(E,R)} \cong -Q_{(V,R)}.$$

Here, the first isomorphism means that the $(|R| - 1)$-dimensional affine lattice $\operatorname{Spin}^c(S^3 - F_G, L) \cong H_1(S^3 - F_G, \mathbf{Z})$ containing $S(F_G)$ has a $\mathbf{Z}$-affine identification with a certain hyperplane in $\mathbf{Z}^R$ so that the image of $S(F_G)$ is $Q_{(E,R)}$. The second isomorphism means that the two sets are translates of each other in $\mathbf{Z}^R$; this is quoted from [13, Theorem 8.3] to show that it hardly matters whether we pick E or V to play the role of the vertices in our hypergraph.

Both sets that appear in Theorem 1.1 can be viewed as multi-variable polynomials and have representations in determinant form. The theorem is proved by showing that a suitable sequence of elimination steps transforms the 'enhanced adjacency matrix' of [13] (which is a large matrix with simple monomial entries) into the Turaev torsion (a smaller matrix with entries obtained as Fox derivatives) that appears in [5]. It would be very interesting to see if the relationship between the two matrices is a special case of some more general phenomenon.

The statement of Theorem 1.1 may seem obscure, but in fact it has some far-reaching consequences. Firstly, as $Q_{(E,R)}$ is easy to compute, and since the support $S(F_G)$ completely determines $SFH(S^3 - F_G, L_G)$, we obtain a simple algorithm for determining the SFH of complements of Seifert surfaces given by the median construction on a bipartite graph. (Proposition 4.3 illustrates the usefulness of this

[1] This slightly deviates from notation in [13], where $Q_{\mathcal{H}}$ stood for the convex hull of the set of hypertrees.

approach.) According to Hirasawa–Sakuma [7] and Banks [2], every minimal genus Seifert surface of a non-split, prime, special alternating link arises in this manner.

Together with the Spin^c-refined Murasugi and connected sum formulas obtained by using [12, Proposition 5.4] in the proofs of [10, Corollary 8.8] and [9, Proposition 9.15], we can also easily compute SFH for Seifert surfaces obtained by applying Seifert's algorithm to homogeneous link diagrams [4] (which include all alternating and positive diagrams). We will call such surfaces *standard*. Indeed, all standard surfaces are Murasugi sums and distant unions of standard Seifert surfaces of non-split, prime, special alternating links. When taking the Murasugi sum or distant union F of the Seifert surfaces F_1 and F_2 of the links L_1 and L_2, respectively, and $L = \partial F$, then

$$\mathrm{Spin}^c(S^3 - F, L) \cong \mathrm{Spin}^c(S^3 - F_1, L_1) \times \mathrm{Spin}^c(S^3 - F_2, L_2).$$

In case of a Murasugi sum,

$$SFH(S^3 - F, L, (\mathfrak{s}_1, \mathfrak{s}_2)) \cong SFH(S^3 - F_1, L_1, \mathfrak{s}_1) \otimes SFH(S^3 - F_2, L_2, \mathfrak{s}_2)$$

for every $\mathfrak{s}_i \in \mathrm{Spin}^c(S^3 - F_i, L_i)$, $i = 1, 2$. In particular, notice that

$$S(F) \cong S(F_1) \times S(F_2). \tag{1}$$

On the other hand, if F is the distant union of F_1 and F_2, then using the connected sum formula for sutured manifolds,

$$SFH(S^3 - F, L, (\mathfrak{s}_1, \mathfrak{s}_2)) \cong SFH(S^3 - F_1, L_1, \mathfrak{s}_1) \otimes SFH(S^3 - F_2, L_2, \mathfrak{s}_2) \otimes \mathbf{Z}^2.$$

We again have (1) for the supports, though $(S^3 - F, L)$ is no longer a sutured L-space as the generators of the $\mathbf{Z}^2$ factor lie in different $\mathbf{Z}/2\mathbf{Z}$-gradings.

As our second application, we derive some previously unknown properties of the SFH of standard Seifert surfaces of homogeneous links. We say that $P \subset \mathbf{Z}^d$ is *convex* if P is the intersection of $\mathbf{Z}^d$ with the convex hull (in $\mathbf{R}^d$) of P. One of the first non-trivial facts about $Q_{\mathcal{H}}$ is that it is convex, see [13, Theorem 3.4]. Combining this with (1), we obtain the following.

Corollary 1.2. *If F is a standard Seifert surface of a homogeneous link L, then $S(F)$ is convex.*

In contrast, if F is a Seifert surface obtained by applying Seifert's algorithm to a non-homogeneous link L, the support $S(F)$ need not be convex, even if the sutured Floer homology is supported in a single $\mathbf{Z}/2\mathbf{Z}$ grading. (For examples, see the computations for three-strand pretzel knots in the last section of [5].)

An unpublished theorem of Richard Webb [19] claims that all standard Seifert surfaces F of an alternating link have isomorphic $S(F)$. Thus if L is a special alternating link, $SFH(S^3 - F, L)$, together with the Spin^c-grading, does not depend on the choice of minimal genus Seifert surface F. On the other hand, Altman [1] gives an example of a knot K with distinct minimal genus Seifert surfaces F_1 and F_2 for which $S(F_1)$ is convex and $S(F_2)$ is not. It would be interesting to know whether an alternating link can have non-standard Seifert surfaces whose SFH differs from that of the standard ones, or whether a homogeneous link can have a non-standard Seifert surface F so that $S(F)$ is non-convex.

Apart from convexity, there is another important context into which Theorem 1.1 fits. Hypertrees were defined as part of a project aimed at finding spanning tree models of some orientation-sensitive link invariants, such as the HOMFLY polynomial. Namely, by counting hypertrees appropriately, from $Q_{\mathcal{H}}$ we may read off a

one-variable polynomial invariant $I_{\mathcal{H}}(\xi)$ of the hypergraph $\mathcal{H}$ [13]. This so-called interior polynomial generalizes the partial evaluation $T(x,1)$ of the Tutte polynomial $T(x,y)$ of ordinary graphs. Then, extending a result of Jaeger [8], the second author proposed the following.

Conjecture. *With notation as above, let $P_{L_G}(v,z)$ denote the HOMFLY polynomial of the link L_G. Then the part of P_{L_G} which (after substituting $v=1$) becomes the leading term in the Alexander–Conway polynomial $\nabla_{L_G}(z) = P_{L_G}(1,z)$ is equal to $(vz)^{|R|-1} I_{(V,E)}(v^2)$.*

As E and V play symmetric roles for L_G, this leads us to expect that $I_{(V,E)} = I_{(E,V)}$. Postnikov and the second author conjecture that this is indeed the case for any connected bipartite graph G; and furthermore, that the two polynomials also coincide with the so-called h-vector of some (any) triangulation of another polytope (called root polytope) derived from G. Then, it has already been proved [14] that this h-vector is equivalent to the relevant part of the HOMFLY polynomial. Therefore, the only missing step is purely discrete mathematical.

Now, if the Conjecture holds true, then the part (hereafter called the *top*) of $P_{L_G}(v,z)$ that realizes its maximum z-degree can be read off from either $Q_{(V,E)}$ or $Q_{(E,V)}$. According to Theorem 1.1, these are equivalent to $S(F_{G_E})$ and $S(F_{G_V})$, respectively, where $G_E = \mathrm{Bip}(V,R) = \mathrm{Bip}(R,V)$ and $G_V = \mathrm{Bip}(E,R) = \mathrm{Bip}(R,E)$ are two plane bipartite graphs closely related to our original graph $G = G_R = \mathrm{Bip}(V,E) = \mathrm{Bip}(E,V)$. The three graphs together form a structure called a trinity. See Figure 4 for an example.

In other words, the Conjecture implies that the top of P_{L_G} can be computed from Floer homology. The alert reader will notice that neither F_{G_E} nor F_{G_V} is a Seifert surface for $L_G = L_{G_R}$. It is also among our goals to derive the same HOMFLY coefficients from $S(F_{G_R})$. There are plenty of indications that this should be possible, including the following consequence of Theorem 1.1 and results in [13].

Corollary 1.3. *With the plane bipartite graphs G_R, G_E, G_V and associated surfaces defined as above, we have $|S(F_{G_R})| = |S(F_{G_E})| = |S(F_{G_V})|$ for the corresponding supports.*

This is true despite the fact that the three sets are the lattice points in three polytopes of different dimensions. Corollary 1.3 is inspired by, and can be viewed as an extension of, Tutte's Tree Trinity Theorem [18]. It is also closely related to Postnikov's duality result $|Q_{(V,E)}| = |Q_{(E,V)}|$, see [17].

Murasugi and Przytycki [16] showed that under 'star product' of links, which is essentially Murasugi sum, the top of the HOMFLY polynomial behaves multiplicatively. Thus, for any homogeneous link, the Conjecture implies that coefficients along the top of the HOMFLY polynomial can be derived from Floer homology groups.

The paper is organized as follows. In sections 2 and 3 we review the necessary results about hypergraphs and Floer homology, respectively. Theorem 1.1, along with some corollaries, is established in section 4. Section 5 contains a detailed sample calculation.

2. Hypergraph invariants

In [13], the second author developed a new theory of hypergraph invariants by generalizing the spanning tree polytope and (partially) the Tutte polynomial to that context. Presently, we will only require the first item, the so called hypertree polytope. This was first defined by A. Postnikov [17], who called it the trimmed generalized permutohedron. (In this paper, instead of polytopes, we will only deal with their integer lattice points.) The relevant definitions and facts are as follows.

A *hypergraph* is a pair $\mathcal{H} = (V, E)$, where V is a finite set and E is a finite multiset of non-empty subsets of V. Elements of V are called *vertices* and the elements of E are the *hyperedges*. Bipartite graphs and hypergraphs can be represented by the same type of picture. We formalize this idea in a two-to-one correspondence where each hypergraph $\mathcal{H}$ has an *associated bipartite graph* $\operatorname{Bip}\mathcal{H}$ in which V and E become the two color classes and $e \in E$ and $v \in V$ are connected if and only if $v \in e$. We will always assume that $\operatorname{Bip}\mathcal{H}$ is connected. Conversely, a connected bipartite graph G *induces* two hypergraphs which we call abstract duals. In other words, the abstract dual $\overline{\mathcal{H}} = (E, V)$ of $\mathcal{H}$ is defined by interchanging the roles of its vertices and hyperedges.

Definition 2.1. Let $\mathcal{H} = (V, E)$ be a hypergraph so that its associated bipartite graph $\operatorname{Bip}\mathcal{H}$ is connected. By a *hypertree* in $\mathcal{H}$ we mean a function (vector) $\mathbf{f}\colon E \to \mathbf{N} = \{0, 1, \dots\}$ so that a spanning tree of $\operatorname{Bip}\mathcal{H}$ can be found which has valence $\mathbf{f}(e) + 1$ at each $e \in E$. The set of all hypertrees in $\mathcal{H}$ will be denoted with $Q_{\mathcal{H}}$.

An elementary observation is that all hypertrees lie on the hyperplane

$$\Pi = \left\{ \mathbf{f}\colon E \to \mathbf{N} \;\middle|\; \sum_{e\in E} \mathbf{f}(e) = |V| - 1 \right\} \subset \mathbf{R}^E.$$

Furthermore, it turns out that hypertrees are exactly the integer lattice points of a polytope which is cut out of Π by inequalities of the form $\sum_{e\in E'} \mathbf{f}(e) \le \mu(E')$, where $\varnothing \ne E' \subsetneqq E$. Here μ is defined as follows[2]. Let $\operatorname{Bip}\mathcal{H}\big|_{E'}$ be the bipartite graph with color classes $E' \subset E$ and $\bigcup E' \subset V$, and edges inherited from $\operatorname{Bip}\mathcal{H}$. Let us denote the number of its connected components by $c(E')$. Then, set $\mu(E') = |\bigcup E'| - c(E')$.

For knot theoretical considerations, a case of particular interest is when $\operatorname{Bip}\mathcal{H}$ is a planar graph, i.e., it comes with an embedding in S^2. Such graphs always occur in sets of three, forming a structure called a trinity. Trinities, first investigated by Tutte [18], have many equivalent descriptions; we choose to define them as triangulations of S^2 with a proper three-coloring of the 0-cells (which we will generally call 'points,' with the understanding that some of them may become 'vertices' in a graph or hypergraph). See Figure 1 for an example.

We will use the names red, emerald and violet for the colors, and denote the respective sets of points by R, E and V. Let us color each edge in the triangulation with the color that does not occur among its ends. Then E and V together with the red edges form a bipartite graph that we will call the *red graph* and denote by G_R. Each region (i.e., connected component of the complement) of the red graph contains a unique red point. Likewise, the *emerald graph* G_E has red and violet points, emerald edges, and regions marked with emerald points. Finally, the

[2] If we let $\mu(\varnothing) = 0$ and $\mu(E) = |V| - 1$, we obtain a non-decreasing submodular set function.

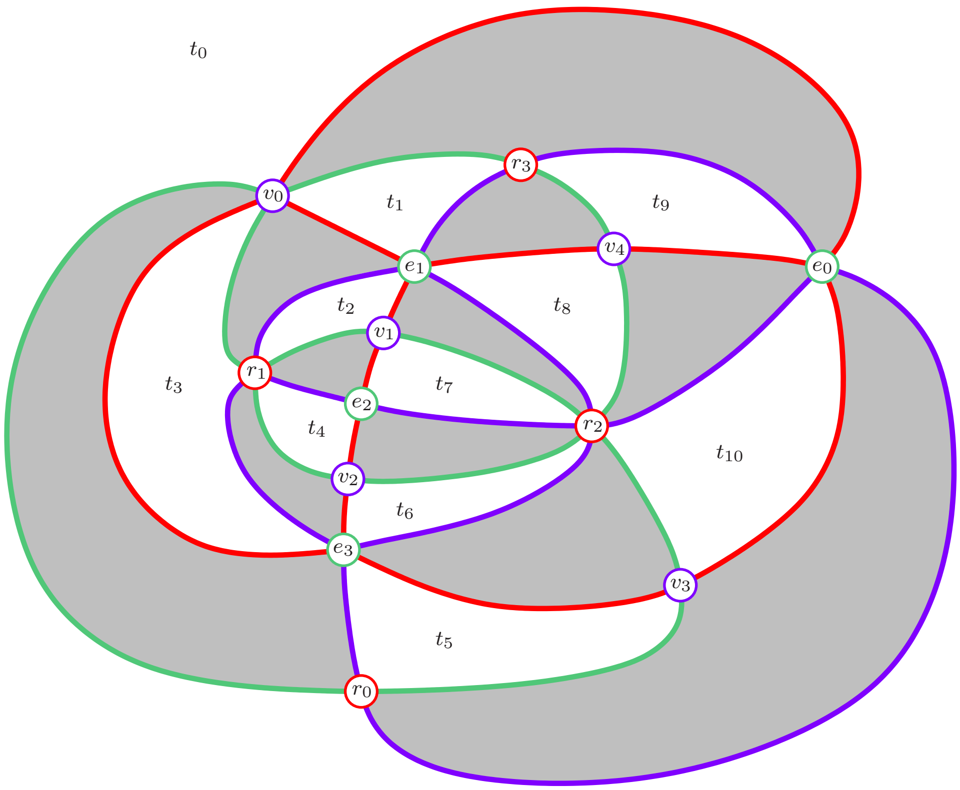

Figure 1. A trinity of plane bipartite graphs.

violet graph contains R and E as vertices, violet edges, and a violet point in each of its regions.

Any one of the six hypergraphs induced by G_R, G_E, or G_V generates the other five (and only those) using two operations. One is abstract duality and the other one is called planar duality. In the latter, hyperedges are retained, but the vertices of the hypergraph are replaced with (points placed in) the regions of its associated plane bipartite graph; the containment relation is defined by adjacency.

In [13, Theorem 8.3], it is established that the hypertree polytopes of planar dual hypergraphs are centrally symmetric. Thus in any trinity, we have $Q_{(V,E)} \cong -Q_{(R,E)} \subset \mathbf{R}^E$, $Q_{(R,V)} \cong -Q_{(E,V)} \subset \mathbf{R}^V$, and

$$Q_{(E,R)} \cong -Q_{(V,R)} \subset \mathbf{R}^R. \tag{2}$$

Notice that each triangle of a trinity is adjacent to exactly one edge and one point of each color. Compared to the orientation of the sphere, the cyclic order of the colors around each triangle may be positive or negative. If two triangles share an edge, these orientations are opposite. Hence the triangles have a black and white checkerboard coloring according to orientation, cf. Figure 1. This coloring can be used to orient the dual graphs G_R^*, G_E^*, and G_V^* (dual in the classical, not in the hypergraph sense). Namely, each edge in these graphs cuts through a black and a white triangle, and we orient it so that its tail end is in black territory.

Next, note that the sets of red edges, emerald edges, violet edges, white triangles, and black triangles all have the same cardinality n. In particular, adjacency defines natural bijections between white triangles and edges of each color. Now, if we apply Euler's formula to the trinity, we get $|R| + |E| + |V| - 3n + 2n = 2$, i.e,

(3) the total number of points exceeds that of the white triangles by 2.

Let us distinguish one white triangle as the *outer* one and label it with t_0. We will label the red, emerald, and violet points adjacent to t_0 with r_0, e_0, and v_0, respectively, and call them the *roots*. According to (3), the non-outer white triangles and non-root points are equal in number, so they form a square adjacency matrix M. We index the rows of M by points and its columns by triangles. This matrix was first investigated by Berman [3] who showed that when we compute the determinant $\det M$, all non-zero expansion terms appear with the same sign. We call these terms the *Tutte matchings* of the trinity.

A Tutte matching is indeed a complete matching of non-root points to adjacent non-outer white triangles. Equivalently, it can be thought of as a collection of edges from G_R^*, G_E^* and G_V^*. Namely, whenever a triangle and a point are matched, we choose the dual edge that cuts through the triangle and ends at the point. It turns out that such a collection is the union of three so called spanning arborescences of G_R^*, G_E^* and G_V^*, respectively, rooted at the respective points adjacent to t_0. (Given an arbitrary vertex q, called root, in a directed graph D, a *spanning arborescence* is a spanning tree of D which contains a directed path from q to any other vertex $p \neq q$ of D.) Each spanning arborescence occurs in relation to exactly one Tutte matching. This fact is the basis of the proof of Tutte's Tree Trinity Theorem [18], i.e., of the claim that G_R^*, G_E^* and G_V^* have the same number of spanning arborescences. (These counts do not depend on the position of the roots either, and of course they are equal to $|\det M|$.)

Definition 2.2. If a non-outer white triangle t_i is adjacent to the red point r_j and the non-root emerald point e_k, then in M, at the intersection of row e_k and column t_i, let us change the entry 1 to r_j. After it becomes a matrix entry, we will think of r_j as an indeterminate associated with the original point. Call the resulting matrix the *enhanced adjacency matrix* and denote it with $M_{r\to e}$.

By varying the colors, altogether six such matrices can be associated to a trinity. According to [13, Theorem 10.5], we may use enhanced adjacency matrices to compute the set of hypertrees in any hypergraph $\mathcal{H}$ as long as $\operatorname{Bip}\mathcal{H}$ is planar.

Proposition 2.3. *In any trinity, for the set of hypertrees in the hypergraph with emerald vertices and red hyperedges, we have*

$$Q_{(E,R)} = \det M_{r\to e}$$

in the following sense. The determinant on the right hand side is a sum of monomials in the indeterminates $r \in R$. Either each monomial has coefficient $+1$, or each has coefficient -1. If we write the exponents in the monomials as vectors, the set we obtain is exactly the left hand side.

Example 2.4. The adjacency matrix associated with the trinity of Figure 1 is

$$M = \begin{array}{c} \\ r_1 \\ r_2 \\ r_3 \\ e_1 \\ e_2 \\ e_3 \\ v_1 \\ v_2 \\ v_3 \\ v_4 \end{array} \!\!\begin{array}{c} \begin{array}{cccccccccc} t_1 & t_2 & t_3 & t_4 & t_5 & t_6 & t_7 & t_8 & t_9 & t_{10} \end{array} \\ \begin{pmatrix} 0 & 1 & 1 & 1 & 0 & 0 & 0 & 0 & 0 & 0 \\ 0 & 0 & 0 & 0 & 0 & 1 & 1 & 1 & 0 & 1 \\ 1 & 0 & 0 & 0 & 0 & 0 & 0 & 0 & 1 & 0 \\ 1 & 1 & 0 & 0 & 0 & 0 & 0 & 1 & 0 & 0 \\ 0 & 0 & 0 & 1 & 0 & 0 & 1 & 0 & 0 & 0 \\ 0 & 0 & 1 & 0 & 1 & 1 & 0 & 0 & 0 & 0 \\ 0 & 1 & 0 & 0 & 0 & 0 & 1 & 0 & 0 & 0 \\ 0 & 0 & 0 & 1 & 0 & 1 & 0 & 0 & 0 & 0 \\ 0 & 0 & 0 & 0 & 1 & 0 & 0 & 0 & 0 & 1 \\ 0 & 0 & 0 & 0 & 0 & 0 & 0 & 1 & 1 & 0 \end{pmatrix} \end{array}.$$

Its determinant is 11. One of its enhancements is as follows.

$$M_{r\to e} = \begin{array}{c} \\ r_1 \\ r_2 \\ r_3 \\ e_1 \\ e_2 \\ e_3 \\ v_1 \\ v_2 \\ v_3 \\ v_4 \end{array} \!\!\begin{array}{c} \begin{array}{cccccccccc} t_1 & t_2 & t_3 & t_4 & t_5 & t_6 & t_7 & t_8 & t_9 & t_{10} \end{array} \\ \begin{pmatrix} 0 & 1 & 1 & 1 & 0 & 0 & 0 & 0 & 0 & 0 \\ 0 & 0 & 0 & 0 & 0 & 1 & 1 & 1 & 0 & 1 \\ 1 & 0 & 0 & 0 & 0 & 0 & 0 & 0 & 1 & 0 \\ r_3 & r_1 & 0 & 0 & 0 & 0 & 0 & r_2 & 0 & 0 \\ 0 & 0 & 0 & r_1 & 0 & 0 & r_2 & 0 & 0 & 0 \\ 0 & 0 & r_1 & 0 & r_0 & r_2 & 0 & 0 & 0 & 0 \\ 0 & 1 & 0 & 0 & 0 & 0 & 1 & 0 & 0 & 0 \\ 0 & 0 & 0 & 1 & 0 & 1 & 0 & 0 & 0 & 0 \\ 0 & 0 & 0 & 0 & 1 & 0 & 0 & 0 & 0 & 1 \\ 0 & 0 & 0 & 0 & 0 & 0 & 0 & 1 & 1 & 0 \end{pmatrix} \end{array}. \tag{4}$$

The determinant of the latter is $r_0r_1^2 + r_0r_1r_2 + r_1^2r_2 + r_0r_2^2 + r_1r_2^2 + r_2^3 + r_0r_1r_3 + r_1^2r_3 + r_0r_2r_3 + r_1r_2r_3 + r_2^2r_3$. If we interpret this formula as in Proposition 2.3, we obtain the picture in Figure 2 for the set $Q_{(E,R)}$ of hypertrees.

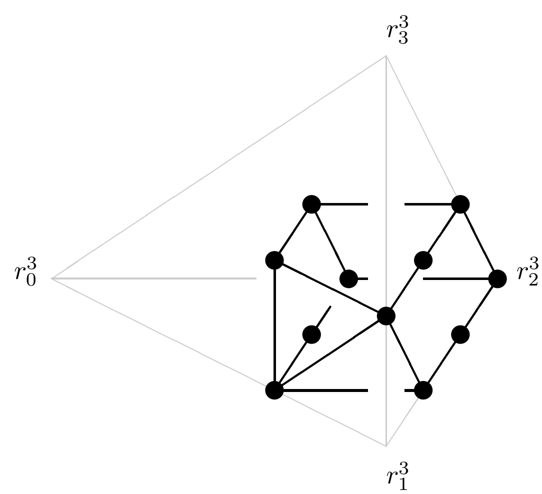

Figure 2. The eleven hypertrees in a hypergraph and their convex hull.

3. Decategorified sutured Floer homology

Sutured Floer homology [9] is an invariant of balanced sutured manifolds. A *sutured manifold* (M, γ) is an oriented three-manifold M, together with an oriented, null-homologous multicurve γ (the *sutures*) on ∂M, see [6]. Since γ is null-homologous, it divides $\partial M - \gamma$ into two pieces R_+ and R_-, with the property that R_+ lies on one side of each curve in γ, and R_- lies on the other. (Note that $R_\pm$ need not be connected.) The condition that (M, γ) is *balanced* means that

(i) $\chi(R_+) = \chi(R_-)$,
(ii) every component of ∂M contains at least one suture and
(iii) M has no closed components.

The sutured manifolds we consider in this paper all arise from the following construction. Suppose that $L \subset S^3$ is an oriented link, and that F is a Seifert surface for L. Let us thicken F slightly to $F \times [-\varepsilon, \varepsilon] \subset S^3$, and let M_F be the closure of its complement. The link L is a subset of ∂M_F, and the pair (M_F, L) is a balanced sutured manifold. Note that both subsurfaces $R_\pm$ are homeomorphic to $\operatorname{int} F$. Thus in this context, we will prefer to use the notation $R_+ = F_+ = F \times \{\varepsilon\}$ and $R_- = F_- = F \times \{-\varepsilon\}$.

When L is an alternating link and F is a minimal genus Seifert surface of L, the sutured Floer homology groups $SFH(M_F, L)$ are completely determined by their Euler characteristic according to [5, Corollary 6.6]. The main result of [5] identifies this Euler characteristic with a certain Turaev torsion $\tau(M_F, L)$. For our purposes, $\tau(M_F, L)$ is best viewed as an element of the group ring $\mathbf{Z}[H_1(M_F; \mathbf{Z})]$ which is well defined up to multiplication by a unit in the group ring.

Let now $G = G_R$ be the red graph of a trinity. As we saw in the previous section, any connected plane bipartite graph uniquely arises in this way. Namely, color the edges of G in red and its two color classes in emerald and violet; place a red point in each region of G and make the appropriate emerald and violet connections between these new points and the old ones. In what follows, let us assume that G is 2-connected, i.e., that it has no cut vertices.

We use the so called median construction to associate the alternating link L_G to G. I.e., along the boundary of each region of G, we first connect the midpoints of consecutive edges by disjoint simple curves. There are exactly two ways to specify over- and undercrossing information at the midpoints themselves so that the union of these curves becomes an alternating link. We use the convention of Figure 3. We also place a positive spin (as in a small counterclockwise spinning top) at each violet point and a negative spin at each emerald point. The link L_G inherits an orientation from the spins as shown in Figure 3 so that its diagram becomes positive. Seifert circles of the diagram correspond to the emerald and violet points so that they are not nested in one another. Hence L_G is a special alternating link, and in fact, any positive special alternating link arises as the result of this construction. (Changing one or both of our choices to the opposite, i.e., mirroring and/or reversing L_G, does not make any major difference.)

By repeating our construction for the other two colors, we end up associating three distinct special alternating links to our trinity. See Figure 4 for an example. These links are of course closely related; see, for instance, Corollary 4.2.

Our construction is such that G is recovered as the Seifert graph of L_G. Hence, if we apply Seifert's construction to the diagram of L_G, we obtain a Seifert surface

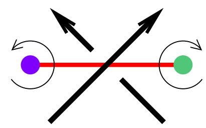

Figure 3. The two strands of L_G crossing an edge of G.

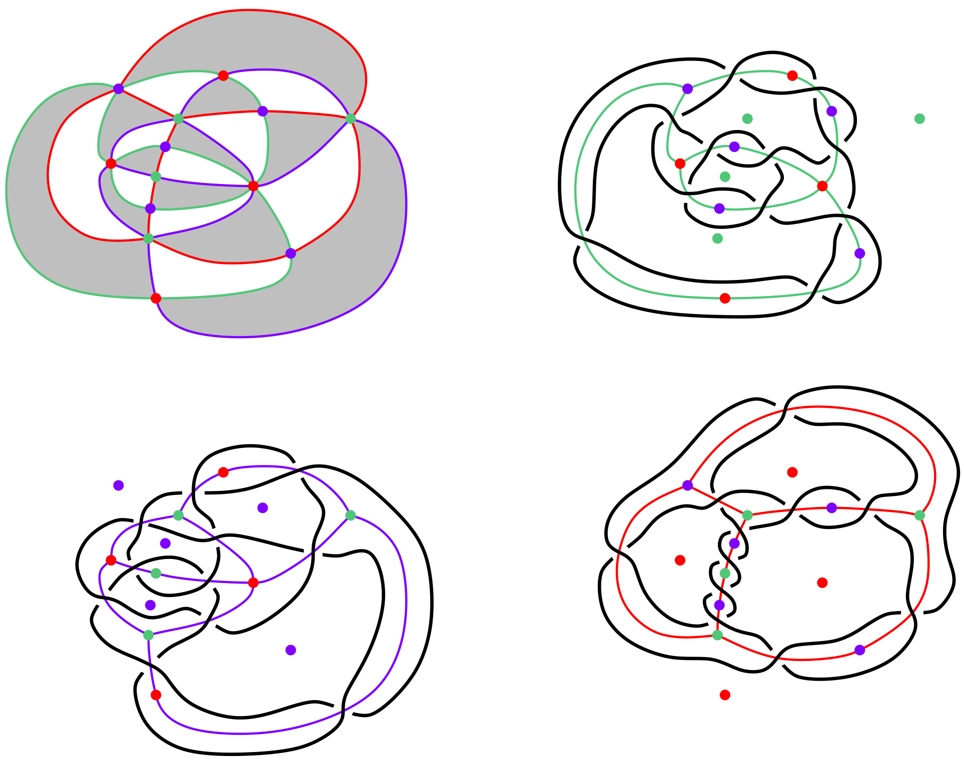

Figure 4. The bipartite graphs of a trinity and the associated special alternating links.

F_G which deformation retracts onto G. Let $M_G = M_{F_G}$ be the complement of this surface. It is easy to see that M_G is a handlebody of genus $|R| - 1$. We are interested in understanding the group $SFH(M_G, L_G)$. Since L_G is alternating, it suffices to study the torsion $\tau(M_G, L_G)$. We now recall from [5] how to compute $\tau(M, \gamma)$ in the case when R_- is connected and M is a handlebody of genus g.

First, we choose a system of co-oriented compressing disks $A_1, \ldots, A_g \subset M$ so that when we cut M along the A_i, the result is a ball. We also fix a basepoint $p \in R_-$ disjoint from the A_i. These data determine a specific isomorphism between $\pi_1(M, p)$ and the free group generated by elements $a_1, \ldots, a_g$. Namely, if c is a loop based at p, we can isotope c so it is transverse to the A_i. Then the word associated to c is obtained by traversing c and recording either an a_i or an a_i^{-1} (depending on the sign of intersection) each time we pass through A_i.

Since (M, γ) is balanced, $\chi(R_-) = \frac{1}{2}\chi(\partial M) = 1 - g$. It follows that $\pi_1(R_-, p)$ is a free group on g generators. Choose a set of generators for $\pi_1(R_-, p)$ and consider their images $W_1, \ldots, W_g \in \pi_1(M, p) \cong \langle a_1, \ldots, a_g \rangle$.

Proposition 3.1. [5, Prop. 5.1] *If M is a handlebody and R_- is connected, then, up to multiplication by a unit, we have*

$$\tau(M,\gamma) \sim \det(|d_{a_i} W_j|),$$

where d_{a_i} denotes the Fox free derivative with respect to a_i and $|\cdot|\colon \mathbf{Z}[\pi_1(M)] \to \mathbf{Z}[H_1(M)]$ is the abelianization.

Example 3.2. Let us choose G to be the red bipartite graph G_R of Figure 4. One way to compute the corresponding Turaev torsion is as follows. Please refer to Figure 6. Our basepoint p will be the push-off of v_0 on the side of F facing the viewer. We fix loops on that side F_- of the surface that go counterclockwise once around the boundary of the region marked with r_1, clockwise around r_0, and counterclockwise around r_3. (The second loop appears in the figure as a counterclockwise path around the outside contour of G_R.)

Our compressing disks correspond to the regions r_1, r_2, and r_3. We co-orient each toward the center of the sphere containing the diagram. (Our figures are drawn from a viewpoint which is outside of the sphere.) For the corresponding free group generators we will use the same symbols r_j.

With these conventions, the three loops that we described above yield the words

$$r_1r_2^{-1}r_1r_2^{-1}r_1r_3^{-1}, \quad r_1r_0^{-1}r_2r_0^{-1}, \quad \text{and} \quad r_3r_2^{-1}r_3r_0^{-1},$$

respectively. Note that we also counted intersections with the region r_0, which did not contribute a compressing disk. In other words, $r_0 = 1$ but we will keep the symbol r_0 around as its presence helps the formalism in the proof of Theorem 1.1. Finally, the Turaev torsion is

$$\begin{vmatrix} 1+r_1r_2^{-1}+r_1^2r_2^{-2} & 1 & 0 \\ -r_1r_2^{-1}-r_1^2r_2^{-2} & r_1r_0^{-1} & -r_3r_2^{-1} \\ -r_1^3r_2^{-2}r_3^{-1} & 0 & 1+r_3r_2^{-1} \end{vmatrix} = r_0^{-1}r_1 + r_0^{-1}r_1^2r_2^{-1} + r_0^{-1}r_1^3r_2^{-2} \tag{5}$$

$$+r_0^{-1}r_1r_2^{-1}r_3 + r_0^{-1}r_1^2r_2^{-2}r_3 + r_0^{-1}r_1^3r_2^{-3}r_3 + r_1^3r_2^{-3} + r_1r_2^{-1} + r_1^2r_2^{-2} + r_1r_2^{-2}r_3 + r_1^2r_2^{-3}r_3.$$

The reader may check that (5) agrees with a monomial $(r_0^{-1}r_1r_2^{-3})$ times the second determinant of Example 2.4. Our main result says that this is not a coincidence.

4. The main result

Due to Propositions 2.3 and 3.1, we may re-state Theorem 1.1 in the following equivalent form.

Theorem 4.1. *Let G be a 2-connected plane bipartite graph (with color classes E and V) and let us realize it as the red graph $G = G_R$ of a trinity. Let the positive special alternating link L_G, Seifert surface F_G and handlebody M_G be associated to G as above. Then, the Turaev torsion $\tau(M_G, L_G)$ is, up to multiplication by a monomial, equal to the determinant of the enhanced adjacency matrix $M_{r\to e}$.*

By writing ‘equal’ above, we assume various identifications through which both determinants become polynomials in indeterminates corresponding to the red points of the trinity. For $\det M_{r\to e}$ this occurs naturally; for $\tau(M_G, L_G)$ it is made explicit below. The proof is not deep but complicated. In the next section, we carry out a concrete computation based on the same method. The reader may wish to study that first or to read it parallel to the proof.

Proof. We are going to describe a very specific way of computing the Turaev torsion, along with an equally specific way of manipulating the enhanced adjacency matrix so that eventually the two determinants are shown to coincide up to a monomial factor. Let us fix an outer white triangle t_0, with adjacent points (roots) r_0, e_0, and v_0 as before. Other points will be labeled with $r_1, \ldots, r_{|R|-1}$, $e_1, \ldots, e_{|E|-1}$, and $v_1, \ldots, v_{|V|-1}$. All additional choices will be dictated by an arbitrarily fixed Tutte matching. I.e., we break the symmetry by singling out one expansion term in $\det M_{r\to e}$.

The Turaev torsion: We compute $\tau(M_G, L_G)$ using the following procedure. First, let us choose compressing disks for M_G the same way as in Example 3.2: Let S^2 denote the sphere containing G, and let us fix an 'outside viewpoint' (which is used to draw our diagrams) and a 'center'. Connect these two points by a path through r_0 and thicken it slightly into a 3-ball. We may think of M_G as this 3-ball with $|R| - 1$ one-handles attached so that each handle passes through a non-root red point. For each $j = 1, 2, \ldots, |R| - 1$, there is an obvious disk contained in S^2, centered at r_j, which is the co-core to one of these handles. We co-orient each disk toward the center of S^2. When the j'th compressing disk is identified with a free group generator, we will write r_j for the latter as well.

Our loops in F_- will be based at $(v_0, -\varepsilon)$. Here, we assume that the thickening of $F = F_G$ has been parametrized so that near the midpoint of the edge κ of t_0 that connects e_0 and v_0, it is F_- that faces the region r_0.

Next, fix a spanning arborescence A in G^* rooted at r_0. As we explained in Section 2, A assigns an adjacent non-outer white triangle to every non-root red point. We choose the labels of these triangles so that t_j is assigned to r_j for all $j = 1, 2, \ldots, |R| - 1$, i.e., that the unique edge of A pointing toward r_j reaches r_j through t_j.

Let now $\Gamma \subset G$ denote the dual tree of A. Note that Γ contains the edge κ because t_0 is not matched to any point. For all j, if we add the dual of the edge of A pointing toward r_j (suppose it has endpoints e^* and v^*) to Γ, a unique cycle is created. We describe it as a sequence λ_j of edges of G that starts at v_0, follows the unique path in Γ to v^*, contains the edge v^*e^* as the next entry, finally returns from e^* to v_0 along the unique path that exists in Γ. In Figure 5 we indicate the two sequences of edges that, along with v^*e^*, make up the loop. Note that, in addition to the point v_0 appearing twice, it is possible for the first (leftmost) several edges to agree, in reverse order, with the last (rightmost) several edges. Other than these coincidences, the edges in λ_j, and hence the white triangles adjacent to them, are all different (in fact, it will sometimes be more useful to think of λ_j as a sequence of triangles rather than of edges) but there may be repetitions among the red points adjacent to those white triangles. In particular, both r_j and r_0 may occur several times.

It is easy to see that the loops λ_j serve as free generators for $\pi_1(G, v_0)$ and hence their push-offs to F_- freely generate $\pi_1(F_-)$. Let us proceed to the word W_j, $j = 1, 2, \ldots, |R| - 1$, in the letters $r_0, r_1, \ldots, r_{|R|-1}$, that is derived from λ_j. (Here the letter r_0 will be used to keep track of intersections with the region r_0. We do this just to preserve symmetry. In the free group, $r_0 = 1$.) As L_G is alternating, the exponents $+1$ and -1 alternate in W_j. Our conventions regarding the thickened surface have been set so that F_- faces the observer near violet points, while near emerald points we see F_+. Hence in W_j the first letter has exponent $+1$, the last

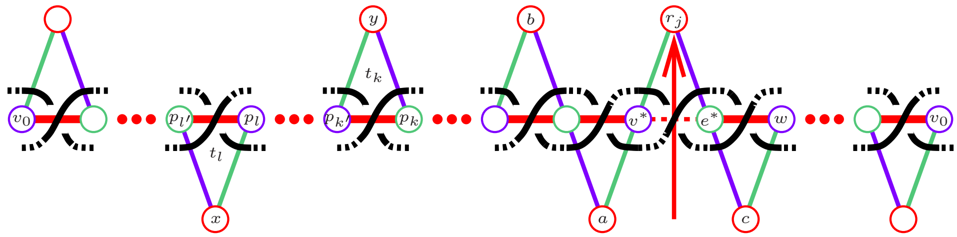

Figure 5. Schematic image of the loop λ_j corresponding to the non-root red point r_j.

has -1, and the edge v^*e^* contributes r_j^{+1}. Highlighting that contribution, let us write $W_j = U_j r_j Z_j$.

When we consider the Fox derivatives of W_j with respect to $r_1, \dots, r_{|R|-1}$, we see that every letter in W_j that is different from $r_0^{\pm 1}$ contributes exactly one monomial to exactly one Fox derivative. Namely, if the red point x appears on the right side of the path (cf. Figure 5) then the contribution is

$$-W^x x^{-1} \text{ to } \partial W_j / \partial x,$$

and a red point y on the left side contributes

$$W^y \text{ to } \partial W_j / \partial y.$$

Here, W^z denotes the part of W_j that precedes the letter z. (This notation is sloppy because z may appear several times in W_j and thus there can be several different W^z's; yet we hope that no confusion will arise.) Our task in the next part of the proof is to arrive at the same monomials in an entirely different way.

Manipulating the enhanced adjacency matrix: We will carry out a sequence of elimination steps on $M_{r\to e}$ inspired by the proof of the Tree Trinity Theorem. We choose a *deconstruction order* $<$ of the points $e_1, \dots, e_{|E|-1}, v_1, \dots, v_{|V|-1}$, by which we mean an order so that the smallest point is a vertex of valence 1 in Γ, then the second smallest is a vertex of valence 1 in the tree that remains if we erase the first vertex and its adjacent edge from Γ, and so on. After removing all non-root vertices in this manner, only the edge κ remains of Γ. For ease of exposition, we will assign a second label to non-root emerald and violet points so that

$$\{\, e_1, \dots, e_{|E|-1}, v_1, \dots, v_{|V|-1} \,\} = \{\, p_{|R|} > p_{|R|+1} > \cdots > p_{n-2} > p_{n-1} \,\}.$$

Here, $n-1 = |R| + |E| + |V| - 3$ is the number of non-root points in the trinity.

The deconstruction order can be used to match non-outer white triangles to the non-root emerald and violet vertices in a one-to-one fashion. The non-root red vertices have already been matched to triangles by the arborescence A and we will not use those triangles again, so that our construction will result in a Tutte matching. The tree Γ contains an edge if and only if the white triangle adjacent to the edge has not been matched to a red point. For the emerald or violet point p_{n-1} having valence 1 in Γ means that all but one of the adjacent white triangles have been matched to red points, so that there is only one choice left. We match that triangle to p_{n-1}. A similar unique choice of a triangle exists for p_{n-2} and so on. We complete the labeling of the white triangles so that the process matches the point p_i with the triangle t_i for each $i = |R|, \dots, n-1$.

The same matching can be described without reference to the deconstruction order as follows: given a non-root point p_i in Γ, the tree has a unique edge adjacent

to it which is such that its other endpoint is closer to κ than p_i is. The white triangle adjacent to this edge is t_i.

From our assumptions on the labeling it follows that if we list the rows and columns of $M_{r\to e}$ in the orders $r_1, \ldots, r_{|R|-1}, p_{|R|}, \ldots, p_{n-1}$ and $t_1, \ldots, t_{n-1}$, respectively, then no zeros appear along the main diagonal and the bottom right $(n-|R|)\times(n-|R|)$ block is upper triangular. Indeed, if $i \geq |R|$, then the red edge of the triangle t_i is in Γ and p_i is the endpoint of this edge which is farther away in Γ from κ. Therefore the other emerald or violet point of t_i is larger than p_i in the deconstruction order.

We will use the $n-|R|$ diagonal entries of this block one by one, from the bottom up, as pivots and at each stage we will perform elementary column operations to eliminate non-zero entries to the left of the pivot. By our remark on upper triangularness, these operations only affect the first $|R|-1$ columns. After elimination, the upper left $(|R|-1)\times(|R|-1)$ block B is such that its determinant differs from $\det M_{r\to e}$ only by a monomial factor, namely the product of the pivots. (In fact the factor is the hypertree in (E,R), written as a monomial, which is associated to the chosen arborescence/Tutte matching.) Therefore it suffices to show that for each $j = 1, \ldots, |R|-1$, the j'th column of B (indexed by the triangle t_j) coincides with U_j^{-1} times the j'th column (indexed by the word W_j) of the Turaev torsion.

Why the two determinants are equal: We will start with a rough description of the effect of our elimination steps and fill in some details later. It suffices to concentrate on just one arbitrary column, say the j'th. In the original enhanced adjacency matrix, the j'th column contains three non-zero entries: 1 in the j'th row which corresponds to the summand U_j in $\partial W_j/\partial r_j$; another 1 in the row indexed by v^*; and r_j in the row indexed by e^*. If e^* or v^* is a root, then one of the latter two is missing. During the elimination process, the number of non-zero entries in the bottom $n-|R|$ positions never increases: it stays two for a while, then goes down to one and eventually to zero. (Or else, it stays one for a while and then becomes zero.)

It is best to think of what is happening in the j'th column as two superimposed, *left and right processes* LP and RP, one for each section of λ_j before and after the edge v^*e^*. (If e^* or v^* is a root, then the corresponding process is empty.) Each process has a non-zero monomial entry, called the *can*, in one of the bottom $n-|R|$ positions which it moves gradually upward until it disappears (as in 'kicking the can down the road'). The can is not constant in the process. In each elimination step, if it affects the j'th column, then one of the two processes takes a step. In that step, the presence of the two (or one) other non-zero entries in the column of the pivot results in the following:

(1) A new non-zero monomial entry (can) is created in one of the lower $n-|R|$ positions of the j'th column. It is higher up than the entry which is eliminated in the step. If the column of the pivot belongs to a white triangle which is adjacent to e_0 or v_0, then this development does not occur and the process terminates.
(2) A new summand (contribution) is added to one of the entries in the upper $|R|-1$ positions of the j'th row. If the column of the pivot belongs to a white triangle adjacent to r_0, then no contribution occurs.

It is also not hard to see that the sequence of pivots for LP and RP starts in the rows indexed by v^* and e^*, respectively, and that the rows of other pivots are

indexed by the emerald and violet points along λ_j that occur as we move toward v_0 along the respective paths. In particular, emerald pivots (equal to some r_i) and violet pivots (equal to 1) alternate in LP as well as in RP. If at either end of λ_j the point adjacent to v_0 is e_0, then the corresponding process ends after the pivot which is in the row of the other violet neighbor of e_0 along λ_j. It is also possible for the two processes to merge after a while as edges and white triangles at the beginning and end of λ_j coincide. After this happens, the cans of LP and RP occur in the same position as a sum of two monomials.

Finally, we need to examine the monomials (cans and contributions) in (1) and (2) above in more concrete terms. Please refer to Figure 5 for notation. Let us first consider the left process LP and the stage when the pivot is the (k,k)-entry y, eliminating the can C^y in the position (k,j). The new can is $-y^{-1}C^y$ and it is in the row indexed by $p_{k'}$. A contribution of $-y^{-1}C^y$ is added to the j'th entry in the row indexed by y. Let now the pivot be the (l,l)-entry 1 and denote the corresponding can by C^x. In this case the new can is $-xC^x$ and it is in the row indexed by $p_{l'}$. A contribution of $-C^x$ is added to the j'th entry in the row indexed by x.

From this it is clear that the sequence of cans for LP is 1, $-a$, $b^{-1}a$, and so on so that C^y is -1 times the product (with alternating exponents) of red points (labels) along λ_j between p_k and v^* and C^x is described similarly but without the negative sign. Then if we look at the contributions $-y^{-1}C^y$ and $-C^x$ of the previous paragraph, we see that if we multiply them by U_j, we get W^y and $-W^x x^{-1}$, respectively, just as we expected and exactly where we expected them.

A similar analysis applies to the right process RP. There, the first can is r_j in the row of e^*, the next one is $-c^{-1}r_j$ (note that the first pivot is c) in the row indexed by w and so on. The entry 1 in the (j,j)-position plays the role of first contribution, then the second one is $-c^{-1}r_j$ in the row indexed by c and so on. After multiplying with U_j, these also conform to our expected values. □

Having established Theorem 1.1, Corollary 1.3 is now immediate: $|S(F_G)|$ is the number of hypertrees in (E,R), but that is the same (by Proposition 2.3) as $|\det M|$ of the 'un-enhanced' adjacency matrix M of the trinity. That number (the number of Tutte matchings) is clearly color-independent.

Let us recall that if F is of minimal genus, then $\sum_{\mathfrak{s}} \chi(SFH(M_F, L, \mathfrak{s}))$ is the leading coefficient of the Alexander polynomial Δ_L, cf. [5, Lemma 6.4] and [10, Theorem 1.5]. (Note that Δ and Conway's version ∇ have the same leading coefficient.) Thus, in our class of examples, $|S(F_G)|$ is the leading coefficient of Δ_{L_G}, and we also obtain the following result.

Corollary 4.2. *The determinant of the adjacency matrix, i.e., the number of Tutte matchings, is the leading coefficient in the Alexander polynomial of any of the three alternating links associated to the trinity.*

This last fact has a more direct proof [14] using the Tree Trinity Theorem [18] and Kauffman's state model [15] for the Alexander polynomial. We now prove Corollary 1.2.

Proof. First, suppose F_G is a standard Seifert surface of a special alternating link L_G, so that $S(F_G) \cong Q_{(E,R)}$. By [13, Theorem 3.4], $Q_{(E,R)}$ is cut out by a system of linear inequalities in $\mathbf{Z}^R$, so it is clearly convex.

Next, suppose F is a standard Seifert surface of a homogeneous link. It is well known that any such F is a Murasugi sum of standard Seifert surfaces for special alternating links. Now (1), along with the fact that the product of convex sets is convex, proves the desired result. □

As another application of Theorem 1.1, we analyze the following situation. Let the edge ε of the 2-connected plane bipartite graph G be adjacent to the regions r_1 and r_2. Let G' be the graph in which ε is replaced with a path of three edges. Then the handlebodies M_G and $M_{G'}$ have a natural identification so that we can think of the supports $S(F_G)$ and $S(F_{G'})$ as subsets of the same affine space over $H_1(M_G; \mathbf{Z})$. In that group, let ε^* denote the homology class of a meridian (in S^3) of ε.

Proposition 4.3. *With the above conventions, $S(F_{G'}) \cong S(F_G) \cup (S(F_G) + \varepsilon^*)$, meaning that the two sides differ by a translation.*

For the convex hulls of the supports, the statement is that $\operatorname{Conv}(S(F_{G'}))$ is the Minkowski sum of $\operatorname{Conv}(S(F_G))$ and a certain line segment. Note that our main example is an instance of G', which explains the 'elongated' shape of the polytope in Figure 2 in the direction from r_1^3 to r_2^3.

Proof. We will prove the relevant claim on sets of hypertrees and leave it to the reader to work out the various identifications. Let E and V denote the color classes of G, and let $E' = E \cup \{e^*\}$ and $V' = V \cup \{v^*\}$ be the corresponding color classes in G'. Both G and G' have the same set R of regions. Then, we claim that

$$Q_{(E',R)} = (Q_{(E,R)} + \mathbf{i}_{\{r_1\}}) \cup (Q_{(E,R)} + \mathbf{i}_{\{r_2\}}),$$

where the $\mathbf{i}_{\{r_i\}}$ are standard generators in $\mathbf{Z}^R$ (indicator functions of singleton sets).

To see this, note that any hypertree $\mathbf{f}$ in (E,R) induces two hypertrees in (E',R) via increasing by 1 the value of $\mathbf{f}$ either at r_1 or at r_2. Indeed, these have obvious spanning trees (in $\operatorname{Bip}(E',R)$) realizing them which are built from a realization (in $\operatorname{Bip}(E,R)$) of $\mathbf{f}$ by adding either the edge r_1e^* or the edge r_2e^*.

To establish the converse, it suffices to show that any hypertree $\mathbf{g}$ in (E',R) has a realization that is of valence one at e^*. If the realization Γ of $\mathbf{g}$ is not such, then e^* is a valence two point in it. Let e denote the emerald endpoint of ε. Then r_1e and r_2e are edges in $\operatorname{Bip}(E',R)$, but at most one of them can be an edge in Γ. If one, say r_1e, is in Γ, then remove r_2e^* from Γ and replace it with r_2e to get the realization of $\mathbf{g}$ with the desired property. If neither r_1e nor r_2e is in Γ, then add r_1e to Γ and kill the resulting cycle by removing its other edge adjacent to r_1. If this was r_1e^*, we are done; otherwise, apply the previous step. □

5. A sample calculation

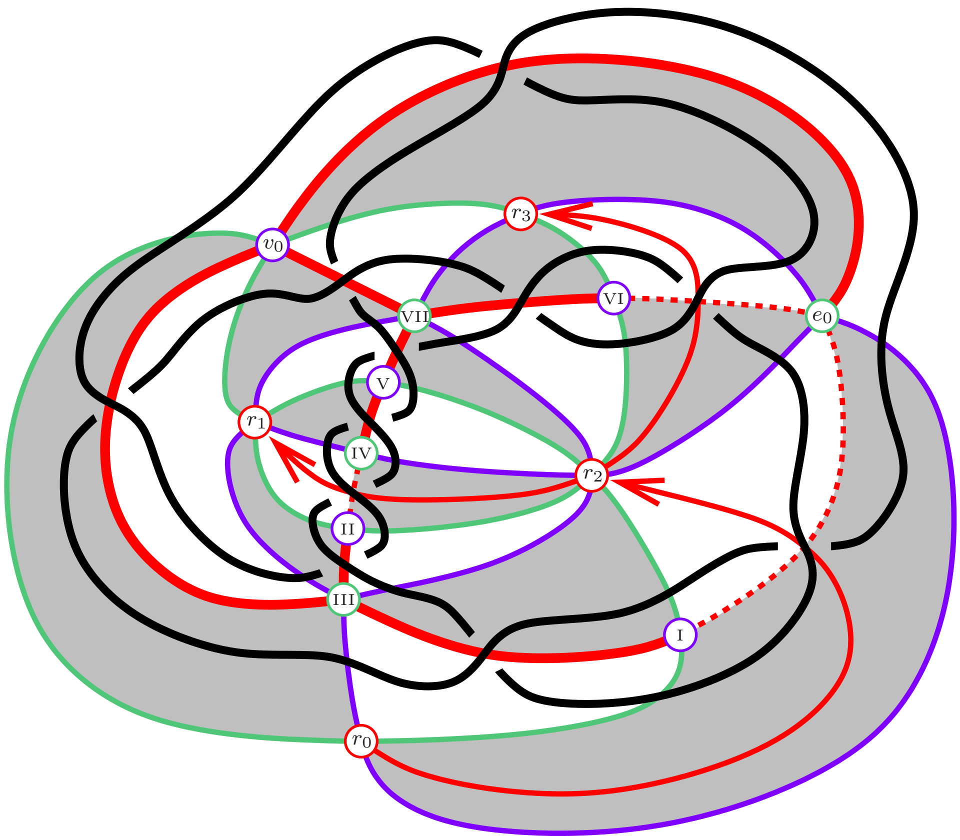

Figure 6. The spanning arborescence $A \subset G_R^*$, its dual tree $\Gamma \subset G_R$, and a deconstruction order for the latter.

We will show explicit reduction steps on the enhanced adjacency matrix in our main running example. The computation will use the spanning arborescence (of G_R^*) indicated in Figure 6. We also fix the deconstruction order $v_3 < v_2 < e_3 < e_2 < v_1 < v_4 < e_1$ as shown in the figure. For better visibility, we have rearranged the rows and columns of the matrix (4) to reflect this order *and* the Tutte matching determined by the arborescence: it now appears as the main diagonal. (Thus we see that the chosen arborescence corresponds to the hypertree/monomial $r_1 r_2 r_3$ of Example 2.4.) We briefly indicate the p-labels that appear in the proof of Theorem 1.1, but we *did not* re-label the white triangles. The signs of all expansion terms in the determinant are still positive, but this is not just by coincidence any more, rather by design. Note how the bottom right 7×7 submatrix is already upper triangular at the start.

In each of the seven steps below, we use the encircled pivot to clear out non-zero entries to its left. Each column of the top left 3×3 block that remains at the end is equal to a monomial times the corresponding column of the determinant (5). As the computation in Example 3.2 was carried out using the procedure in the first half of the proof of Theorem 1.1, this indeed illustrates the correctness of our method.

$$\begin{array}{r} \\ r_1 \\ r_2 \\ r_3 \\ p_4 = e_1 \\ p_5 = v_4 \\ p_6 = v_1 \\ p_7 = e_2 \\ p_8 = e_3 \\ p_9 = v_2 \\ p_{10} = v_3 \end{array}
\begin{array}{c} \begin{array}{cccccccccc} t_4 & t_{10} & t_9 & t_1 & t_8 & t_2 & t_7 & t_3 & t_6 & t_5 \end{array} \\
\begin{pmatrix}
1 & 0 & 0 & 0 & 0 & 1 & 0 & 1 & 0 & 0 \\
0 & 1 & 0 & 0 & 1 & 0 & 1 & 0 & 1 & 0 \\
0 & 0 & 1 & 1 & 0 & 0 & 0 & 0 & 0 & 0 \\
0 & 0 & 0 & r_3 & r_2 & r_1 & 0 & 0 & 0 & 0 \\
0 & 0 & 1 & 0 & 1 & 0 & 0 & 0 & 0 & 0 \\
0 & 0 & 0 & 0 & 0 & 1 & 1 & 0 & 0 & 0 \\
r_1 & 0 & 0 & 0 & 0 & 0 & r_2 & 0 & 0 & 0 \\
0 & 0 & 0 & 0 & 0 & 0 & 0 & r_1 & r_2 & r_0 \\
1 & 0 & 0 & 0 & 0 & 0 & 0 & 0 & 1 & 0 \\
0 & 1 & 0 & 0 & 0 & 0 & 0 & 0 & 0 & 1
\end{pmatrix} \end{array};$$

$$\begin{array}{r} \\ r_1 \\ r_2 \\ r_3 \\ e_1 \\ v_4 \\ v_1 \\ e_2 \\ e_3 \\ v_2 \\ v_3 \end{array}
\begin{array}{c} \begin{array}{cccccccccc} t_4 & t_{10} & t_9 & t_1 & t_8 & t_2 & t_7 & t_3 & t_6 & t_5 \end{array} \\
\begin{pmatrix}
1 & 0 & 0 & 0 & 0 & 1 & 0 & 1 & 0 & 0 \\
0 & 1 & 0 & 0 & 1 & 0 & 1 & 0 & 1 & 0 \\
0 & 0 & 1 & 1 & 0 & 0 & 0 & 0 & 0 & 0 \\
0 & 0 & 0 & r_3 & r_2 & r_1 & 0 & 0 & 0 & 0 \\
0 & 0 & 1 & 0 & 1 & 0 & 0 & 0 & 0 & 0 \\
0 & 0 & 0 & 0 & 0 & 1 & 1 & 0 & 0 & 0 \\
r_1 & 0 & 0 & 0 & 0 & 0 & r_2 & 0 & 0 & 0 \\
0 & -r_0 & 0 & 0 & 0 & 0 & 0 & r_1 & r_2 & r_0 \\
1 & 0 & 0 & 0 & 0 & 0 & 0 & 0 & 1 & 0 \\
0 & 0 & 0 & 0 & 0 & 0 & 0 & 0 & 0 & 1
\end{pmatrix} \end{array};$$

$$\begin{array}{r} \\ r_1 \\ r_2 \\ r_3 \\ e_1 \\ v_4 \\ v_1 \\ e_2 \\ e_3 \\ v_2 \\ v_3 \end{array}
\begin{array}{c} \begin{array}{cccccccccc} t_4 & t_{10} & t_9 & t_1 & t_8 & t_2 & t_7 & t_3 & t_6 & t_5 \end{array} \\
\begin{pmatrix}
1 & 0 & 0 & 0 & 0 & 1 & 0 & 1 & 0 & 0 \\
-1 & 1 & 0 & 0 & 1 & 0 & 1 & 0 & 1 & 0 \\
0 & 0 & 1 & 1 & 0 & 0 & 0 & 0 & 0 & 0 \\
0 & 0 & 0 & r_3 & r_2 & r_1 & 0 & 0 & 0 & 0 \\
0 & 0 & 1 & 0 & 1 & 0 & 0 & 0 & 0 & 0 \\
0 & 0 & 0 & 0 & 0 & 1 & 1 & 0 & 0 & 0 \\
r_1 & 0 & 0 & 0 & 0 & 0 & r_2 & 0 & 0 & 0 \\
-r_2 & -r_0 & 0 & 0 & 0 & 0 & 0 & r_1 & r_2 & r_0 \\
0 & 0 & 0 & 0 & 0 & 0 & 0 & 0 & 1 & 0 \\
0 & 0 & 0 & 0 & 0 & 0 & 0 & 0 & 0 & 1
\end{pmatrix} \end{array};$$

$$\begin{array}{r} \\ r_1 \\ r_2 \\ r_3 \\ e_1 \\ v_4 \\ v_1 \\ e_2 \\ e_3 \\ v_2 \\ v_3 \end{array}
\begin{array}{c} \begin{array}{cccccccccc} t_4 & t_{10} & t_9 & t_1 & t_8 & t_2 & t_7 & t_3 & t_6 & t_5 \end{array} \\
\begin{pmatrix}
1 + r_1^{-1} r_2 & r_1^{-1} r_0 & 0 & 0 & 0 & 1 & 0 & 1 & 0 & 0 \\
-1 & 1 & 0 & 0 & 1 & 0 & 1 & 0 & 1 & 0 \\
0 & 0 & 1 & 1 & 0 & 0 & 0 & 0 & 0 & 0 \\
0 & 0 & 0 & r_3 & r_2 & r_1 & 0 & 0 & 0 & 0 \\
0 & 0 & 1 & 0 & 1 & 0 & 0 & 0 & 0 & 0 \\
0 & 0 & 0 & 0 & 0 & 1 & 1 & 0 & 0 & 0 \\
r_1 & 0 & 0 & 0 & 0 & 0 & r_2 & 0 & 0 & 0 \\
0 & 0 & 0 & 0 & 0 & 0 & 0 & r_1 & r_2 & r_0 \\
0 & 0 & 0 & 0 & 0 & 0 & 0 & 0 & 1 & 0 \\
0 & 0 & 0 & 0 & 0 & 0 & 0 & 0 & 0 & 1
\end{pmatrix} \end{array};$$

$$
\begin{array}{cc}
 & \begin{array}{cccccccccc} t_4 & t_{10} & t_9 & t_1 & t_8 & t_2 & t_7 & t_3 & t_6 & t_5 \end{array} \\
\begin{array}{c} r_1 \\ r_2 \\ r_3 \\ e_1 \\ v_4 \\ v_1 \\ e_2 \\ e_3 \\ v_2 \\ v_3 \end{array} &
\begin{pmatrix}
1+r_1^{-1}r_2 & r_1^{-1}r_0 & 0 & 0 & 0 & 1 & 0 & 1 & 0 & 0 \\
-1-r_2^{-1}r_1 & 1 & 0 & 0 & 1 & 0 & 1 & 0 & 1 & 0 \\
0 & 0 & 1 & 1 & 0 & 0 & 0 & 0 & 0 & 0 \\
0 & 0 & 0 & r_3 & r_2 & r_1 & 0 & 0 & 0 & 0 \\
0 & 0 & 1 & 0 & 1 & 0 & 0 & 0 & 0 & 0 \\
-r_2^{-1}r_1 & 0 & 0 & 0 & 0 & 1 & 1 & 0 & 0 & 0 \\
0 & 0 & 0 & 0 & 0 & 0 & r_2 & 0 & 0 & 0 \\
0 & 0 & 0 & 0 & 0 & 0 & 0 & r_1 & r_2 & r_0 \\
0 & 0 & 0 & 0 & 0 & 0 & 0 & 0 & 1 & 0 \\
0 & 0 & 0 & 0 & 0 & 0 & 0 & 0 & 0 & 1
\end{pmatrix}
\end{array};
$$

$$
\begin{array}{cc}
 & \begin{array}{cccccccccc} t_4 & t_{10} & t_9 & t_1 & t_8 & t_2 & t_7 & t_3 & t_6 & t_5 \end{array} \\
\begin{array}{c} r_1 \\ r_2 \\ r_3 \\ e_1 \\ v_4 \\ v_1 \\ e_2 \\ e_3 \\ v_2 \\ v_3 \end{array} &
\begin{pmatrix}
1+r_1^{-1}r_2+r_2^{-1}r_1 & r_1^{-1}r_0 & 0 & 0 & 0 & 1 & 0 & 1 & 0 & 0 \\
-1-r_2^{-1}r_1 & 1 & 0 & 0 & 1 & 0 & 1 & 0 & 1 & 0 \\
0 & 0 & 1 & 1 & 0 & 0 & 0 & 0 & 0 & 0 \\
r_2^{-1}r_1^2 & 0 & 0 & r_3 & r_2 & r_1 & 0 & 0 & 0 & 0 \\
0 & 0 & 1 & 0 & 1 & 0 & 0 & 0 & 0 & 0 \\
0 & 0 & 0 & 0 & 0 & 1 & 1 & 0 & 0 & 0 \\
0 & 0 & 0 & 0 & 0 & 0 & r_2 & 0 & 0 & 0 \\
0 & 0 & 0 & 0 & 0 & 0 & 0 & r_1 & r_2 & r_0 \\
0 & 0 & 0 & 0 & 0 & 0 & 0 & 0 & 1 & 0 \\
0 & 0 & 0 & 0 & 0 & 0 & 0 & 0 & 0 & 1
\end{pmatrix}
\end{array};
$$

$$
\begin{array}{cc}
 & \begin{array}{cccccccccc} t_4 & t_{10} & t_9 & t_1 & t_8 & t_2 & t_7 & t_3 & t_6 & t_5 \end{array} \\
\begin{array}{c} r_1 \\ r_2 \\ r_3 \\ e_1 \\ v_4 \\ v_1 \\ e_2 \\ e_3 \\ v_2 \\ v_3 \end{array} &
\begin{pmatrix}
1+r_1^{-1}r_2+r_2^{-1}r_1 & r_1^{-1}r_0 & 0 & 0 & 0 & 1 & 0 & 1 & 0 & 0 \\
-1-r_2^{-1}r_1 & 1 & -1 & 0 & 1 & 0 & 1 & 0 & 1 & 0 \\
0 & 0 & 1 & 1 & 0 & 0 & 0 & 0 & 0 & 0 \\
r_2^{-1}r_1^2 & 0 & -r_2 & r_3 & r_2 & r_1 & 0 & 0 & 0 & 0 \\
0 & 0 & 0 & 0 & 1 & 0 & 0 & 0 & 0 & 0 \\
0 & 0 & 0 & 0 & 0 & 1 & 1 & 0 & 0 & 0 \\
0 & 0 & 0 & 0 & 0 & 0 & r_2 & 0 & 0 & 0 \\
0 & 0 & 0 & 0 & 0 & 0 & 0 & r_1 & r_2 & r_0 \\
0 & 0 & 0 & 0 & 0 & 0 & 0 & 0 & 1 & 0 \\
0 & 0 & 0 & 0 & 0 & 0 & 0 & 0 & 0 & 1
\end{pmatrix}
\end{array};
$$

$$
\begin{array}{cc}
 & \begin{array}{cccccccccc} t_4 & t_{10} & t_9 & t_1 & t_8 & t_2 & t_7 & t_3 & t_6 & t_5 \end{array} \\
\begin{array}{c} r_1 \\ r_2 \\ r_3 \\ e_1 \\ v_4 \\ v_1 \\ e_2 \\ e_3 \\ v_2 \\ v_3 \end{array} &
\begin{pmatrix}
1+r_1^{-1}r_2+r_2^{-1}r_1 & r_1^{-1}r_0 & 0 & 0 & 0 & 1 & 0 & 1 & 0 & 0 \\
-1-r_2^{-1}r_1 & 1 & -1 & 0 & 1 & 0 & 1 & 0 & 1 & 0 \\
-r_3^{-1}r_2^{-1}r_1^2 & 0 & 1+r_3^{-1}r_2 & 1 & 0 & 0 & 0 & 0 & 0 & 0 \\
0 & 0 & 0 & r_3 & r_2 & r_1 & 0 & 0 & 0 & 0 \\
0 & 0 & 0 & 0 & 1 & 0 & 0 & 0 & 0 & 0 \\
0 & 0 & 0 & 0 & 0 & 1 & 1 & 0 & 0 & 0 \\
0 & 0 & 0 & 0 & 0 & 0 & r_2 & 0 & 0 & 0 \\
0 & 0 & 0 & 0 & 0 & 0 & 0 & r_1 & r_2 & r_0 \\
0 & 0 & 0 & 0 & 0 & 0 & 0 & 0 & 1 & 0 \\
0 & 0 & 0 & 0 & 0 & 0 & 0 & 0 & 0 & 1
\end{pmatrix}
\end{array}.
$$

References

[1] Irida Altman, *Sutured Floer homology distinguishes between Seifert surfaces*, arXiv:1012.5904.

[2] Jessica E. Banks, *Minimal Genus Seifert Surfaces for Alternating Links*, arXiv:1106.3180.

[3] K. A. Berman, *A proof of Tutte's trinity theorem and a new determinant formula*, SIAM J. Algebraic Discrete Methods 1 (1980), no. 1, 64–69.

[4] P. R. Cromwell, *Homogeneous links*, J. London Math. Soc. 39 (1989), no. 3, 535–552.

[5] S. Friedl, A. Juhász, and J. Rasmussen, *The decategorification of sutured Floer homology*, arXiv:0903.5287.

[6] D. Gabai, *Foliations and the topology of 3-manifolds*, J. Diff. Geom. 18 (1983), 445–503.

[7] M. Hirasawa and M. Sakuma, *Minimal genus Seifert surfaces for alternating links*, in KNOTS '96 (Tokyo), pp. 383–394, World Sci. Publ., River Edge, NJ, 1997.

[8] F. Jaeger, *Tutte polynomials and link polynomials*, Proc. Amer. Math. Soc. 103 (1988), no. 2, 647–654.

[9] A. Juhász, *Holomorphic discs and sutured manifolds*, Algebr. Geom. Topol. 6 (2006), 1429–1457.

[10] A. Juhász, *Floer homology and surface decompositions*, Geom. Topol. 12 (2008), 299–350.

[11] A. Juhász, *Knot Floer homology and Seifert surfaces*, Algebr. Geom. Topol. 8 (2008), 603–608.

[12] A. Juhász, *The sutured Floer homology polytope*, Geom. Topol. 14 (2010), no. 3, 1303–1354.

[13] T. Kálmán, *A version of Tutte's polynomial for hypergraphs*, arXiv:1103.1057.

[14] T. Kálmán and H. Murakami, *Root polytopes and the Homfly polynomial of alternating links*, in progress.

[15] L. H. Kauffman, *Formal Knot Theory*, Mathematical Notes 30, Princeton Univ. Press, Princeton, NJ, 1983.

[16] K. Murasugi and J. Przytycki, *The skein polynomial of a planar star product of two links*, Math. Proc. Camb. Phil. Soc. 106 (1989), 273–276.

[17] A. Postnikov, *Permutohedra, Associahedra, and Beyond*, Int. Math. Res. Not. 2009, no. 6, 1026–1106.

[18] W. T. Tutte, *The dissection of equilateral triangles into equilateral triangles*, Proc. Cambridge Philos. Soc. 44 (1948), 463–482.

[19] R. Webb, *Alexander polynomials of sutured handlebodies*, Trinity College summer research report, 2009.

Cambridge University
E-mail address: `A.Juhasz@dpmms.cam.ac.uk`

Tokyo Institute of Technology
E-mail address: `kalman@math.titech.ac.jp`
URL: `www.math.titech.ac.jp/~kalman`

Cambridge University
E-mail address: `J.Rasmussen@dpmms.cam.ac.uk`